ACS APPLIED MATERIALS & INTERFACES

Research Article

Cite This: ACS Appl. Mater. Interfaces 2020, 12, 2362−2369

www.acsami.org

One-Step Sublimation and Epitaxial Growth of CdS-Cd Heterogeneous Nanoparticles on S-Doped MoO_2 Nanosheets for Efficient Visible Light-Driven Photocatalytic H_2 Generation

Hui Liu,[†,‡,§] Jiayuan Yu,[§] Yuke Chen,[‡] Ziqian Zhou,[§] Guowei Xiong,[‡] Lili Zeng,[§] Haidong Li,[∥] Zhen Liu,[‡] Lili Zhao,[‡] Jingang Wang,[‡] Benli Chu,[*,†] Hong Liu,[*,‡,⊥] and Weijia Zhou[*,‡,§]

[†]School of Physics and Telecommunication Engineering, South China Normal University, Guangzhou Higher Education Mega Center, Guangzhou, Guangdong 510006, P. R. China

[‡]Collaborative Innovation Center of Technology and Equipment for Biological Diagnosis and Therapy in Universities of Shandong, Institute for Advanced Interdisciplinary Research (iAIR), University of Jinan, Jinan 250022, P. R. China

[§]Guangzhou Key Laboratory for Surface Chemistry of Energy Materials, New Energy Research Institute, School of Environment and Energy, South China University of Technology, Guangzhou Higher Education Mega Center, Guangzhou, Guangdong 510006, P. R. China

[∥]College of Materials Science and Engineering, Qingdao University, Qingdao 266071, P. R. China

[⊥]State Key Laboratory of Crystal Materials, Shandong University, Jinan 250100, P. R. China

Supporting Information

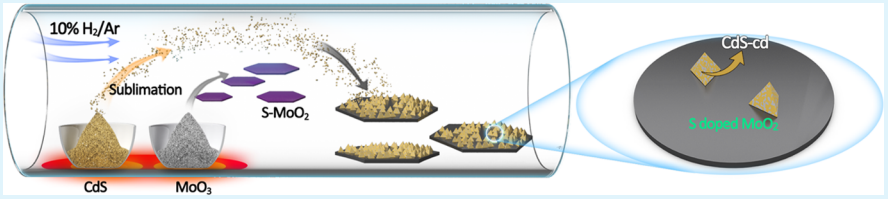

ABSTRACT: As a green, pollution-free, and renewable clean energy source, photocatalytic H_2 production has attracted great attention. Here, epitaxial growth of pyramidal CdS-Cd nanoparticles on S-doped MoO_2 nanosheets (CdS-Cd/S-MoO_2) was prepared by one-step co-sublimation of CdS and MoO_3. The photogenerated electrons of CdS as a photocatalyst are transferred to Cd and S-MoO_2 as co-catalysts for H_2 production, which is observed by surface photovoltage (SPV) under visible light irradiation. At last, the obtained CdS-Cd/S-MoO_2 presented an efficient photocatalytic performance under the visible light (>420 nm) with a prominent H_2 generation rate of as high as 24.98 μmol h^{-1} mg^{-1}, which is 11 times higher than that of the CdS-Cd nanoparticles (2.26 μmol h^{-1} mg^{-1}), and it is superior than that of the CdS (1.51 μmol h^{-1} mg^{-1}).

KEYWORDS: *sublimation, epitaxial growth, heterostructure, photocatalytic hydrogen generation, co-catalyst*

1. INTRODUCTION

At present, environmental problems are getting worse due to the population explosion and industrial development; as a result, energy demand becomes urgent. As a renewable and clean energy source, H_2 production is a hot topic in research. Photocatalytic water splitting for H_2 production is considered to be the most promising way. Since TiO_2 was first reported as a catalyst for photocatalytic water splitting to H_2 production in 1972,[1] semiconductors for photocatalytic H_2 production have been extensively studied.[2−7] Among them, cadmium sulfide (CdS) as a semiconductor with a suitable band gap of 2.4 eV has a good visible light absorption range, and electrical conductivity for photocatalytic H_2 production has drawn intensive attention.[8−12] In the past decades, plenty of modification methods have been widely proposed, including the fabrication of nanostructured CdS,[13] constructing semiconductor heterojunctions,[14−19] and coupling with carbons.[20,21] Shang et al. reported that metal Cd nanosheets with thicknesses ranging around 30−50 nm were transformed into CdS nanoparticles decorated Cd nanosheet heterostructured photocatalysts (CdS NP/Cd NSs) by an oxidation−sulfurization process, which showed significantly enhanced activity in visible light-driven photocatalytic H_2 production because of the electrical conductivity and efficient charge carrier separation among the rectifying Schottky junctions formed between the CdS NP absorbers and Cd NSs.[22]

Co-catalysts, supporting on semiconductor photocatalysts, can greatly improve the activity of the catalysts. It is an effective way to restrain charge carrier recombination.[23−27] It is generally believed that noble metals, such as platinum, can effectively be photodeposited on cadmium sulfide photocatalysts.[28] The obtained quantum efficiency of photocatalytic

Received: September 23, 2019
Accepted: December 17, 2019
Published: December 17, 2019

DOI: 10.1021/acsami.9b17216
ACS Appl. Mater. Interfaces 2020, 12, 2362−2369

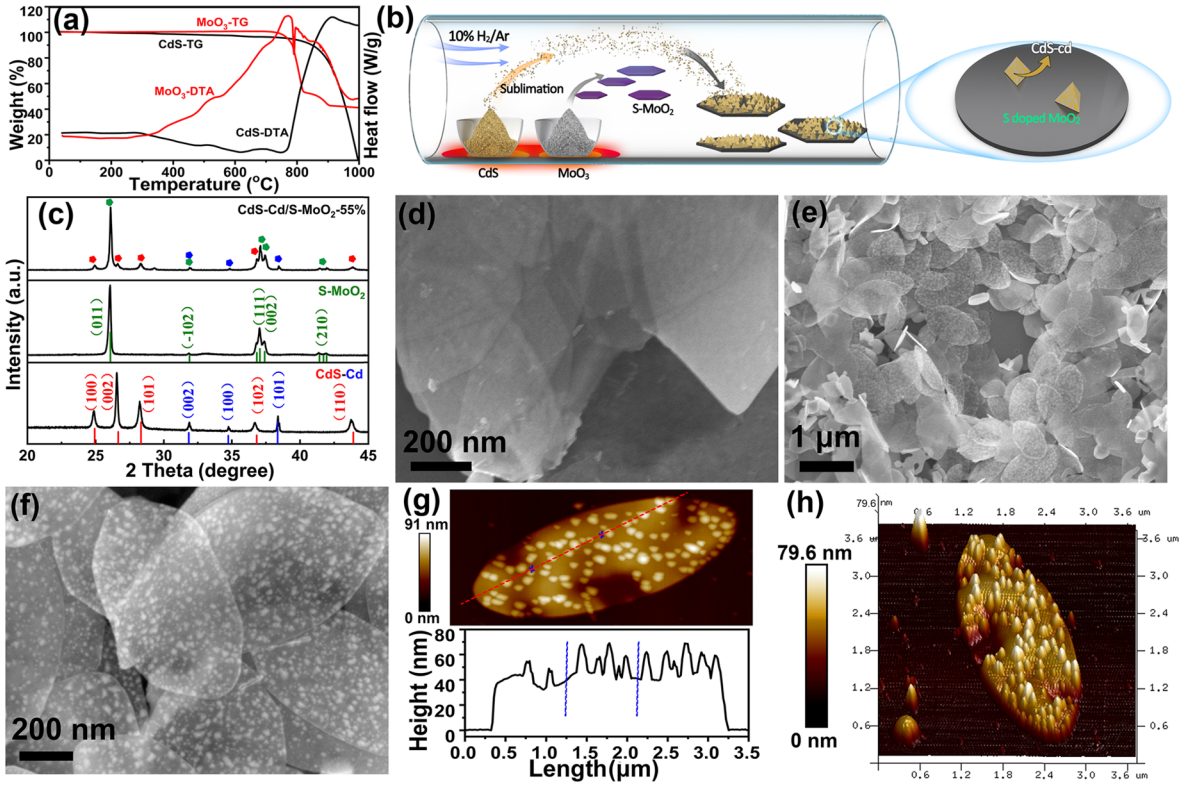

Figure 1. (a) TG/DSC curve of MoO_3 and CdS sublimation. (b) Schematic of the one-step sublimation synthesis of CdS-Cd/S-MoO_2. (c) XRD patterns of CdS-Cd, S-MoO_2, and CdS-Cd/S-MoO_2-55%. FESEM images of (d) S-MoO_2 nanosheets and (e, f) CdS-Cd/S-MoO_2-55%. (g) AFM topography image. (h) 3D diagram of CdS-Cd/S-MoO_2-55%.

H_2 generation is very high due to the promotion of charge separation and the improvement of H_2 production kinetics. Layered transition metal dichalcogenide nanosheets, as another kind of cocatalysts, such as MS_2 (M = W or Mo),[29−33] exhibited remarkable performance toward electrocatalytic H_2 evolution. Chen et al. reported a facile one-pot wet chemical method for the preparation of MS_2-CdS (M = W or Mo) nanohybrids, in which a single-layer MS_2 nanosheet was selectively grown on the surface of the CdS-rich (001). These MS_2-CdS nanohybrids with a large number of active edge sites on the MS_2 layers with a lateral size of 4−10 nm possess enhanced photocatalytic performance under visible light irradiation (>420 nm) and catalytic stability.[34] However, the synthesis of CdS photocatalysts containing non-noble metal co-catalysts on a large scale via green technology is still required.

Consequently, we fabricated CdS-Cd nanopyramid decorated S-doped MoO_2 nanosheets (CdS-Cd/S-MoO_2-55%) by a one-step sublimation of CdS and MoO_3. It is worth noting that the one-step and large scale of the synthesis process were simple and environment-friendly, which avoided producing sulfurous waste liquid and waste gas. The CdS-Cd/S-MoO_2-55% was composed of CdS nanoparticles as photocatalysts and Cd and S-MoO_2 nanosheets as co-catalysts, which showed efficient photocatalytic H_2 generation performance under the visible light (>420 nm). The corresponding H_2 production rate of CdS-Cd/S-MoO_2-55% was 24.98 μmol h^{-1} mg^{-1}, which is 11 times higher than that of the CdS-Cd nanoparticles (2.26 μmol h^{-1} mg^{-1}), and it is superior than that of the CdS (1.51 μmol h^{-1} mg^{-1}). UV−vis absorption spectra and UPS spectra confirmed the enhanced light absorption capability and energy band matching structure of CdS-Cd/S-MoO_2. The photoluminescence spectra and atomic force microscope also confirmed the effective photoelectric charge efferent characteristics between CdS-Cd nanopyramids and S-doped MoO_2 nanosheets.

2. EXPERIMENTAL SECTION

2.1. Materials. All chemicals in this work were of analytical grade and were used without further purification. Cadmium sulfide (CdS), molybdenum trioxide (MoO_3), sodium sulfide nonahydrate ($Na_2S·9H_2O$; AR), and sodium sulfite (Na_2SO_3; AR) were purchased from Sinopharm Chemical Reagents Beijing Co. Ltd.

2.2. Preparation of CdS-Cd Nanoparticle Decorated S-Doped MoO_2 Nanosheets (CdS-Cd/S-MoO_2). CdS powder (30 mg) was put in front of the MoO_3 powder, and both of them were put in the heating area of a tubular furnace. The Ar gas was pumped into the tube to remove air, and then rapidly heated up to 900 °C (20 °C/min). After that, the calcination temperature was kept at 900 °C for 30 min in the atmosphere of 10% H_2/Ar (200 sccm). A large amount of black powder was blown into the low temperature zone (30 °C) of the tubular furnace, which was collected as CdS-Cd nanoparticle decorated S-doped MoO_2 nanosheets (CdS-Cd/S-MoO_2), and the yield was about 80%. Samples (431 mg) were synthesized by increasing the amount of the reactant (300 mg of MoO_3 powder and 300 mg of CdS powder), and the existing morphology and structure can still be maintained, as shown in Figure S1, but the yield will be reduced to about 71.8%. The loading ratio of CdS onto MoO_2 was adjusted by setting the amount of MoO_3 (30 mg) and changing that of CdS (10, 20, 30, and 40 mg). Because CdS and Cd can be dissolved by the concentrated hydrochloric acid, the CdS-Cd loading amounts of the different product were calculated, as shown in Table S1. The samples were named as CdS-Cd/S-MoO_2-15%, CdS-Cd/S-MoO_2-40%, CdS-Cd/S-MoO_2-55%, and CdS-Cd/S-MoO_2-75%. The results were basically consistent with those calculated from EDS element mapping, as shown in Figure S2. In addition, some samples were synthesized for comparison. The pure MoO_2 nanosheets and

DOI: 10.1021/acsami.9b17216
ACS Appl. Mater. Interfaces 2020, 12, 2362−2369

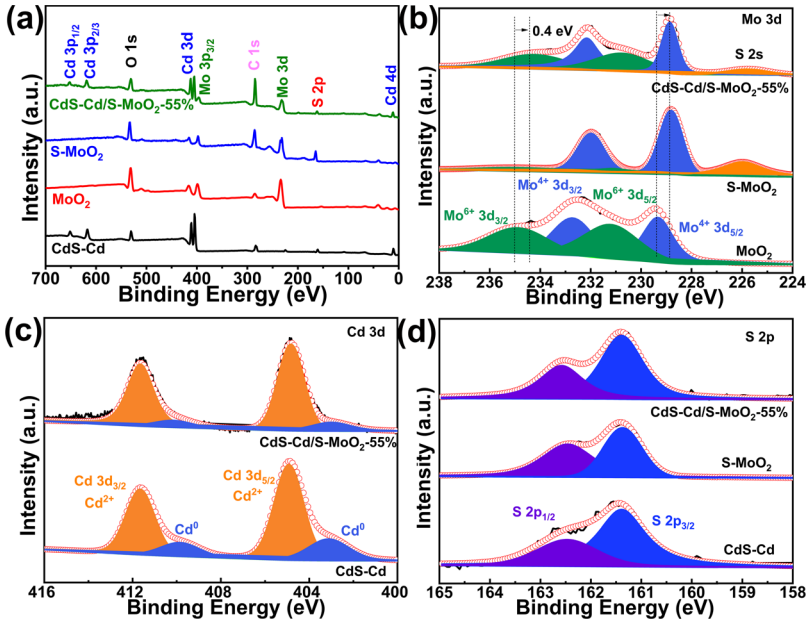

Figure 2. (a) XPS spectra of CdS-Cd, MoO_2, S-MoO_2, and CdS-Cd/S-MoO_2-55%. High-resolution signals of (b) Mo 3d, (c) Cd 3d, and (d) S 2p.

CdS-Cd particles were synthesized without CdS and MoO_3 by the similar process of CdS-Cd/S-MoO_2-55%. The pure CdS particles were synthesized by the similar process of CdS-Cd/S-MoO_2-55%, while the Ar gas was used instead of 10% H_2/Ar. The S-doped MoO_2 nanosheets (S-MoO_2) were prepared in the sublimation of MoO_3 powder with 10% H_2S/Ar gas.

3. RESULTS AND DISCUSSION

As we know, the cadmium sulfide and molybdenum trioxide possessed the sublimation character at high-temperature calcination, which were ~800 °C for CdS and ~790 °C for MoO_3, respectively, confirmed by the thermogravimetric differential scanning calorimeter (TG/DSC) in Figure 1a. The S-doped MoO_2 (S-MoO_2) nanosheets were synthesized by annealing MoO_3 powders with 10% H_2/Ar and 10% H_2S/Ar gas at 900 °C confirmed by XRD (PDF #73-1249; Figure 1c), which possessed characteristic peaks at 18.42, 26, and 37.22° attributed to the (100), (011), and (002) of MoO_2, respectively.[35] The obtained S-MoO_2 exhibited a hexagonal-shape nanosheet with a few micrometers and smooth margins and surfaces (Figure 1d). As shown in Figure S3, the EDS element mapping of Mo, O, and S in S-MoO_2 proved that S successfully doped into MoO_2 nanosheets. The pure MoO_2 nanosheets were prepared by 10% H_2/Ar gas without H_2S, which possessed the similar morphology and crystal structure, as shown in Figure S4. In the absence of MoO_2 nanosheets, the large CdS-Cd blocks were obtained by the same process without regular morphology (1−5 μm; Figure S5). As XRD and SEM images are shown in Figure S6, CdS nanoparticles were synthesized by Ar instead of 10% H_2/Ar, which were aggregated into large blocks. In Figure 1c, the XRD diffraction peaks at 24.9, 26.6, 28.3, 36.8, and 43.9° were attributed to (100), (002), (101), (102), and (110) crystal facets of CdS (PDF #80-0006), respectively, and 31.8, 34.7, and 38.3° were attributed to (002), (100), and (101) crystal facets of metallic Cd (PDF #85-1328), respectively. Because of the similar sublimation temperature of CdS and MoO_3, the hetero-structure of CdS-Cd nanoparticle decorated S-doped MoO_2 nanosheets (CdS-Cd/S-MoO_2-55%) was synthesized during the calcination at 900 °C, which is shown in Figure 1b. When CdS and MoO_3 were simultaneously sublimated in an Ar-H_2 (10% H_2) atmosphere at 900 °C, the hexagonal nanosheets decorated with nanoparticles are observed by FESEM images in Figure 1e,f. The XRD patterns of CdS-Cd/S-MoO_2-55% in Figure 1c showed the characteristic peaks of MoO_2[35] at 18.42, 26, and 37.22°, the characteristic peaks of CdS at 24.9, 26.6, 28.3, 36.8, and 43.9°, and the characteristic peaks of Cd at 31.8, 34.7, and 38.3°. Thus, the nanoparticles on MoO_2 nanosheets were speculated as CdS-Cd composites. The CdS-Cd nanoparticles possessed sizes of 20−60 nm due to the restriction and supporter effect of MoO_2 nanosheets. At last, the loading amount of CdS on MoO_2 nanosheets can be controlled by adjusting the precursor mass ratios between CdS and MoO_3, the FESEM images and XRD results are listed in Figure S7. Like the additional amount of CdS, the sizes of nanoparticles also increase, which were ~5 (CdS-Cd/S-MoO_2-15%), ~10 (CdS-Cd/S-MoO_2-40%), and ~100 nm (CdS-Cd/S-MoO_2-75%). It was important that the CdS-Cd/S-MoO_2 was synthesized on a large scale, which was expediently collected at the end of the quartz tube at room temperature (Figure S8).

Atomic force microscopy (AFM) was used to study the thickness of S-MoO_2 nanosheets and the size of CdS-Cd nanoparticles, as shown in Figure 1g,h. The thickness of the S-MoO_2 nanosheet as a supporter was 30−40 nm. Interestingly, the CdS-Cd nanoparticles were not spherical, which were two-dimensional and triangle flakes in Figure 1g. In the 3D diagram in Figure 1h, we can also see the uniform distribution of pyramid structure particles with widths of ~50 nm and heights of 10−20 nm on a S-MoO_2 nanosheet. Moreover, the AFM image of CdS-Cd/S-MoO_2-75% with large CdS-Cd particles gave a more intuitive evidence of the pyramid structure, which is shown in Figure S9.

According to the results mentioned above, the possible chemical reaction equilibriums were listed as follows. Solid-state MoO_3 was sublimated to gaseous hexavalent molybdenum (eq 1), which was reduced into MoO_2 and then by H_2 (eq 2). The similar process was carried out for CdS. Solid-state CdS was sublimated to gaseous CdS (eq 3), and the CdS was partially reduced into Cd and H_2S by 10% H_2/Ar (eq 4). The

DOI: 10.1021/acsami.9b17216
ACS Appl. Mater. Interfaces 2020, 12, 2362−2369

trace H_2S produced was possible to be doped into MoO_2 nanosheets (S-MoO_2, eq 5) because no MoS_2 was detected by XRD (Figure 1c).

$$MoO_3\ (s) \rightarrow MoO_3\ (g) \quad (1)$$

$$MoO_3\ (g) + H_2 \rightarrow MoO_2\ (s) + H_2O \quad (2)$$

$$CdS\ (s) \rightarrow CdS\ (g) \quad (3)$$

$$CdS + H_2 \rightarrow Cd + H_2S \quad (4)$$

$$MoO_2 + H_2S \rightarrow S - MoO_2 \quad (5)$$

To investigate the surface composition and the electronic states of CdS-Cd, MoO_2, S-MoO_2, and CdS-Cd/S-MoO_2-55%, X-ray photoelectron spectroscopy (XPS) measurement was carried out. The XPS survey spectrum in Figure 2a showed that the Cd, Mo, S, and O elements coexist in CdS-Cd/S-MoO_2-55%. In Figure 2b, for pure MoO_2, the characteristic peaks at 232.9 and 229.2 eV were attributed to the Mo $3d_{3/2}$ and Mo $3d_{5/2}$ of Mo^{4+}, respectively. The oxidation state Mo^{6+} peaks at 235.1 (Mo $3d_{3/2}$) and 231.5 eV (Mo $3d_{5/2}$) were detected due to the oxidation exposed to air.[35] Compared with MoO_2, Mo 3d peaks of S-MoO_2 shifted about 0.4 eV to low binding energy, possibly due to the S−Mo bond.[26,36−38] In addition, the S 2 s peak at 225.7 eV also appeared in S-MoO_2 and CdS-Cd/S-MoO_2-55%. As for CdS-Cd/S-MoO_2-55%, the similar peaks with those of S-MoO_2 were observed, indicating the S doping into MoO_2. As for XPS spectra of CdS-Cd, the four peaks at 411.7 and 404.9 eV and 403.1 and 409.7 eV were attributed to the Cd $3d_{3/2}$ and Cd $3d_{5/2}$ of Cd^{2+} and Cd^0, respectively.[39] As for CdS-Cd/S-MoO_2-55%, the similar peaks fitting to ionic and metallic Cd were also detected (Figure 2c). The high-resolution XPS spectra of the S 2p are displayed in Figure 2d, two characteristic peaks of S $2p_{3/2}$ and S $2p_{1/2}$ in CdS-Cd, S-MoO_2, and CdS-Cd/S-MoO_2-55% were observed.[40] All the above data confirmed the successful synthesis of the CdS-Cd composite with different valences and S doping into MoO_2.

Transmission electron microscopy (TEM) was obtained to further analyze the crystal structure of CdS-Cd/S-MoO_2-55%, as shown in Figure 3. The hexagonal nanosheets as a substrate decorated with uniform nanoparticles were observed, as shown in Figure 3a. The two pieces of CdS-Cd/S-MoO_2-55% nanosheets overlaid together because of the ultimately thin shapes of the materials, which were transparent to an electron beam. It is worth noting that the CdS-Cd nanoparticles possessed the polygonal structure, as shown in Figure 3a,d.

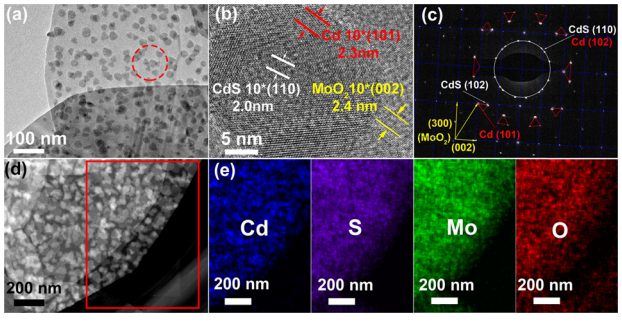

Figure 3. (a, b) (HR)TEM images of CdS-Cd/S-MoO_2-55% with (c) corresponding electron-diffraction pattern. (d, e) EDS mapping of Cd, S, Mo, and O for CdS-Cd/S-MoO_2-55%.

The pyramid shape of CdS-Cd nanoparticles was more clearly observed for CdS-Cd/S-MoO_2-75% with a high loading amount of CdS (Figure S10), which was consistent with the AFM image (Figure S9). The well-defined lattice fringes with a spacing of 0.24 nm were in compliance with the (002) plane of the MoO_2 substrate in Figure 3b. In addition, other lattice fringes with spacings of 0.334 and 0.23 nm agreed well with the (002) crystal planes of CdS and (101) crystal planes of Cd on the same nanoparticle, which implied the heterostructure between CdS and Cd. The electron-diffraction pattern, as displayed in Figure 3c, showed that a set of diffraction spot was consistent with the (002) and (300) planes of MoO_2 in the long range, implying the single-crystal structure of the S-MoO_2 nanosheet. Interestingly, the diffraction spots around the spot of MoO_2 can be connected into a triangle and pointed to the diffraction center and matched with the (102) of CdS and the (101) of Cd, which were consistent with XRD results (Figure 1c), implying that the lattice orientations of CdS-Cd nanopyramids were consistent. This was possible that the epitaxial growth of CdS nanoparticles was induced by the crystal plane of MoO_2 nanosheets with a small lattice mismatch. The similar results have been reported.[41] Moreover, the discontinuous diffraction rings that constituted diffraction spots in pairs were the CdS (110) and the crystal plane of the Cd (102) plane, which also possessed the small lattice mismatch between them and induced growth of the CdS-Cd heterostructure. The element mapping characterization is shown in Figure 3d, which demonstrated that the nanosheets were uniformly composed of Mo, O, Cd and S elements. The Cd element was distributed in particle form, and S, Mo, and O elements were distributed in nanosheet form, which also confirmed that the CdS-Cd nanopyramids were loaded on the S-doped MoO_2 nanosheets. In addition, the element mapping of CdS-Cd/S-MoO_2-75% with a high loading amount of CdS (Figure S10), which was washed by acid to remove CdS-Cd nanoparticles (Figure S11), also demonstrated S doping into MoO_2 nanosheets.

High activity photocatalyst and efficiency co-catalyst have a good effect on the photocatalytic H_2 production system. The UV−vis absorption spectra were used to measure the light absorption capacity and calculate the band gap of CdS, S-MoO_2, and CdS-Cd/S-MoO_2-55%, as shown in Figure 4a,b. It is worth noting the fluctuation of light absorption at 850 nm due to the automatic replacement of light source in a spectrophotometer. For pure CdS nanoparticles, there was a light absorbance at a wavelength of around 575 nm, and the corresponding band gap was about ~2.16 eV.[42] The band gaps of CdS-Cd and S-MoO_2 were measured to be 1.9 and 0.8 eV. The S-MoO_2 obtained had a broad absorption of visible and near-infrared light. The CdS-Cd/S-MoO_2-55% exhibited a flat plot with an enhanced light harvesting at a wavelength beyond 510 nm, which could be attributed to the stronger light absorption and metallic nature of the narrow band of S-MoO_2. The band gap value of CdS-Cd/S-MoO_2-55% calculated was ~1.7 eV, indicating that there was a strong electron coupling between the CdS-Cd polygonal particles and the S-MoO_2 nanosheets, that is, how we can achieve the enhanced visible light absorption.

The semicircle diameter fitted by the EIS Nyquist plots in Figure 4c showed that the CdS-Cd/S-MoO_2-55% offered the highest charge transfer efficiency and confirmed the excellent charge separation between photogenerated electrons and holes.[43] Compared with that in the dark condition, the

DOI: 10.1021/acsami.9b17216
ACS Appl. Mater. Interfaces 2020, 12, 2362−2369

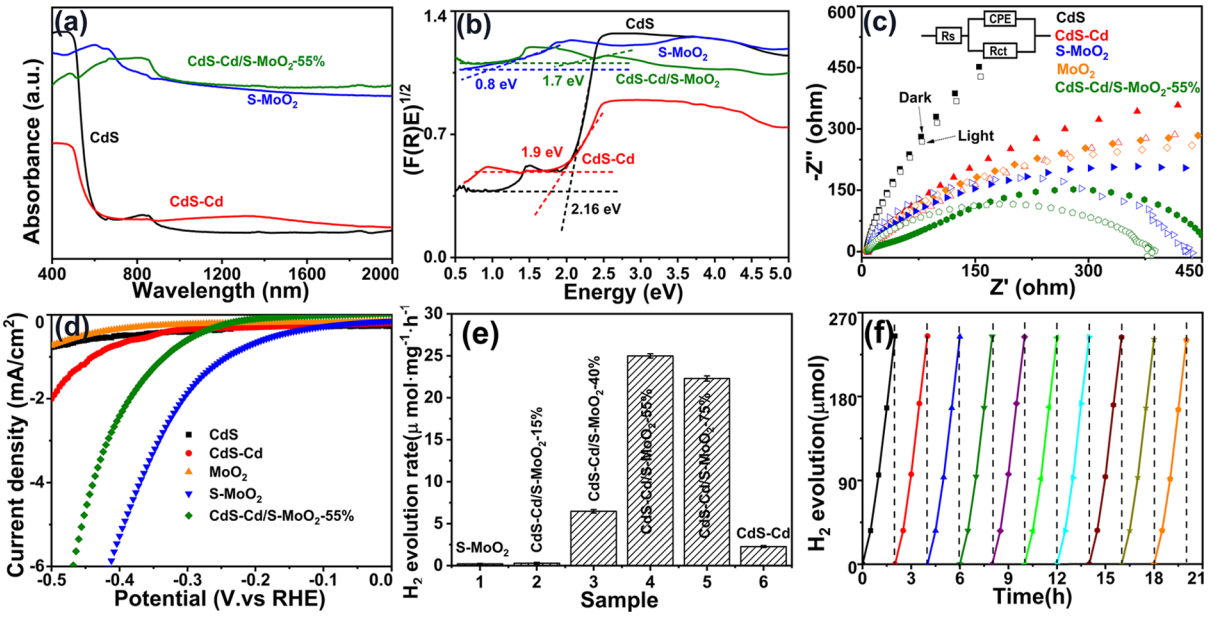

Figure 4. (a) UV−vis absorption spectra, (b) the plots of $(F(R)E)^{1/2}$, and (c) Nyquist plots from electrochemical impedance spectroscopy of CdS, CdS-Cd, S-MoO_2, and CdS-Cd/S-MoO_2-55%. (d) Polarization curves of CdS, CdS-Cd, MoO_2, S-MoO_2, and CdS-Cd/S-MoO_2-55%. (e) H_2 evolution rates of CdS-Cd, S-MoO_2, and different loading of a CdS-Cd/S-MoO_2 light wavelength of >420 nm. (f) Cycling test of the photocatalytic activity of CdS-Cd/S-MoO_2-55%.

charge-transfer resistance (R_{ct}) value of CdS-Cd/S-MoO_2-55% possessed the largest change under visible light illumination, which was consistent with the photoelectrochemical response (Figure S12a), photoluminescence (PL) spectra (Figure S12b), and the fluorescence decay curves (Figure S12c).The above results proved that CdS-Cd nanoparticles and S-MoO_2 nanosheets had a perfect combination to obtain the longer lifetime of photoinduced electron−hole pairs, which confirmed the most efficient photocatalytic system.

To discuss the function of each component in CdS-Cd/S-MoO_2-55%, the electrocatalytic properties of the CdS, CdS-Cd, MoO_2, S-MoO_2, and CdS-Cd/S-MoO_2-55% were evaluated in a 0.5 M H_2SO_4 solution with a three-electrode electrochemical setup, as shown in Figure 4d. The pure CdS and MoO_2 were inert for the hydrogen evolution reaction (HER), and the onset potentials were larger than 500 mV versus RHE. The CdS-Cd had a lower onset potential of about 450 mV versus RHE than that of the CdS, which proved that the Cd was a possible electrocatalyst for HER. The polarization curve of S-MoO_2 showed a lower onset potential of 242 mV versus RHE than that of MoO_2, implying that S doping was beneficial to the improvement of HER activity of MoO_2. Consequently, the HER activity of CdS-Cd/S-MoO_2-55% with an onset potential of 334 mV versus RHE was attributed to Cd and S-MoO_2.

To evaluate the photocatalytic performance of the CdS-Cd/S-MoO_2 system, the photocatalytic H_2 evolution with Na_2S and Na_2SO_3 as hole sacrificial agents under the visible light with a light wavelength of >420 nm was performed (Figure 4e). It is worth noting that the 0.25 M Na_2SO_3 and 0.35 M Na_2S aqueous solutions without photocatalysts were tested with visible light (>420 nm), and no hydrogen was produced. In Figure S13, the photocatalytic hydrogen production performance of CdS, CdS-Cd, and 0.5 wt % Pt/CdS confirmed that the Cd as a co-catalyst promoted the photocatalytic activity of CdS, and the corresponding H_2 evolution rates were 1.51, 2.26, and 2.91 μmol h^{-1} mg^{-1}. In addition, the MoO_2 and S-MoO_2 nanosheets that produced negligible hydrogen values of 0 and 0.21 μmol h^{-1} mg^{-1} (Figure S14) under visible light (>420 nm), respectively, confirmed that the S-MoO_2 possessed weak photocatalytic H_2 production activity. Based on the results above, CdS-Cd/S-MoO_2-55% was composed of the Cd and S-MoO_2 electrocatalysts as cocatalysts with enhanced the electrocatalytic activity, and CdS as a photocatalyst with enhanced light absorption capacity caused the high photocatalytic performance for H_2 production. In addition, Figure 4e shows that the H_2 evolution rate of CdS-Cd/S-MoO_2-55% (24.98 μmol h^{-1} mg^{-1}) is over 11 times higher than that of the CdS-Cd nanoparticles (2.26 μmol h^{-1} mg^{-1}) under the visible light radiation. With the increased loading of CdS, photocatalytic H_2 production performances of CdS-Cd/S-MoO_2 were improved, which were 0.28, 6.47, and 24.98 μmol h^{-1} mg^{-1}. However, by further increasing the CdS loading, the amount of photocatalytic H_2 production decreased to a certain extent, which was 22.29 μmol h^{-1} mg^{-1} of CdS-Cd/S-MoO_2-75%. This implied that the enhanced photocatalytic activity was not only because of the increased amount of CdS as photocatalyst but also because of the intimate interaction between the CdS photocatalyst and S-MoO_2 co-catalysts.

In Figure 4f, the 20 h photocatalytic tests of CdS-Cd/S-MoO_2-55% showed no significant deactivation during 10 runs of experiments, which confirmed the good photocatalytic stability. The XRD (Figure S15a), XPS curve of Mo 3d (Figure S15b), and Cd 3d (Figure S15c) of CdS-Cd/S-MoO_2-55% before and after the photocatalytic reaction showed no significant change of the crystal structure and surface elements, which confirmed the structure stability. The corresponding apparent quantum efficiency (AQE) and H_2 evolution amount of the different photocatalysts under 420 nm and CdS-Cd/S-MoO_2-55% under different homogeneous lights (420, 500, 600, and 650 nm) are listed in Figure S16 a,b, the highest AQE value was 64.9% for CdS-Cd/S-MoO_2-55% under 420 nm. In addition, the photocatalytic hydrogen evolution activity of

DOI: 10.1021/acsami.9b17216
ACS Appl. Mater. Interfaces 2020, 12, 2362−2369

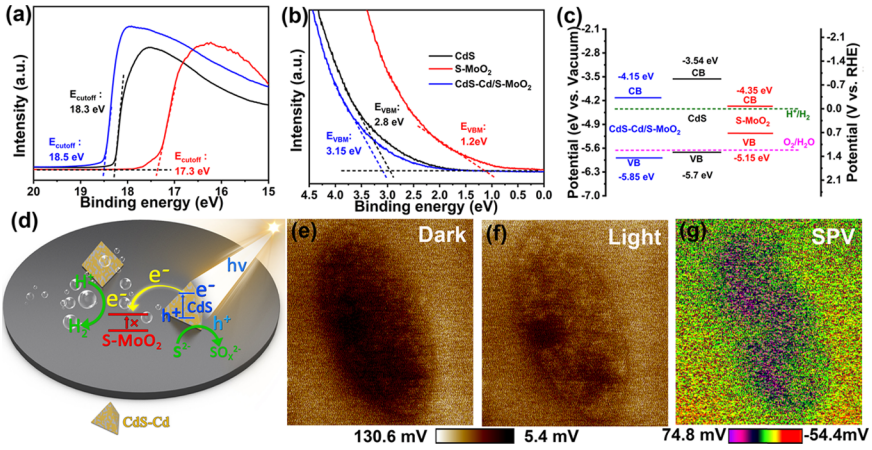

Figure 5. UPS spectra of (a) secondary edge and (b) low energy onset regions. (c) Corresponding band structure diagram of CdS, S-MoO_2, and CdS-Cd/S-MoO_2-55%. (d) Proposed mechanism for the energy band matching and charge separation of CdS-Cd/S-MoO_2 under visible light irradiation. (e–g) KPFM image and the surface potential distribution in the (e) dark, (f) under light irradiation at λ = 532 nm, and (g) SPV of the CdS-Cd/S-MoO_2-55%.

various catalysts in other particles is listed in Table S2, which can be seen that the sample has good performance.

To better understand the detailed band structure of CdS-Cd/S-MoO_2, the ultraviolet photoelectron spectra (UPS) of CdS, S-MoO_2, and CdS-Cd/S-MoO_2-55% were recorded, the secondary electron cutoff (E_{cutoff}) and valence band maximum (E_{VBM}) are shown in Figure 5a,b, respectively. The valence band maximum (VBM) energy levels were obtained by calculating the UPS data from the following formula[12,44]

VBM = $h\nu$ − (E_{cutoff} − E_{VBM})where $h\nu$ (21.22 eV) was the incident photon energy and E_{VBM} was the onset relative to the Fermi level (E_F) of the Si substrate. The work functions (ϕ) calculated by E_{cutoff} were 2.92, 3.92, and 2.72 eV for CdS, S-MoO_2, and CdS-Cd/S-MoO_2-55%, respectively. The valence band energies (E_{VB}) were also determined to be 5.7, 5.12, and 5.85 eV, respectively. Furthermore, due to the $E_g = E_{VB} - E_{CB}$, combined with the UV–vis result, the conduction band energies (E_{CB}) of CdS, S-MoO_2, and CdS-Cd/S-MoO_2-55% were thus determined to be 3.54, 4.32, and 4.15 eV, respectively. Based on UPS and UV–vis data, the energy band diagram is found in Figure 5c. The CdS with an energy gap of 2.16 eV possessed a valence band position at 5.7 eV versus vacuum and a conduction band (CB) at 3.54 eV versus vacuum, which was similar with the reported result.[45] After being loaded onto S-MoO_2 nanosheets, the conduction band of CdS-Cd/S-MoO_2-55% moved down to 4.15 eV versus vacuum for H_2 production and the reduced energy gap of 1.7 eV, which increased light absorption. Besides, the calculated conduction band of S-MoO_2 was close to 0 eV versus RHE. However, the photocatalytic activity of S-MoO_2 was negligible, which was thought to act as a co-catalyst. As the result above, photocatalytic H_2 generation mechanism can be seen in Figure 5d. Under visible light irradiation, the photogenerated electrons of CdS were transferred to co-catalysts of Cd and S-MoO_2 nanosheets, which reduced hydrogen ions to H_2 molecules. The photogenerated holes of CdS were consumed by the sacrificial agent of Na_2S and Na_2SO_3.

To confirm the electron transfer path, the surface potential images of CdS-Cd/S-MoO_2-55% in dark and under light were carried out by the photoassisted Kelvin probe force microscopy (KPFM) technique,[46] as shown in Figure 5e,f, respectively. The KPFM image showed a clear difference in potential distribution between CdS-Cd particles and the S-MoO_2 nanosheet region in dark and under 532 nm light irradiation. The difference value of surface photovoltage (SPV) between the nanosheet and the particles increased after light irradiation.[47] It can be seen in Figure 5g that the high potential was distributed on the pyramidal CdS-Cd particles, and the low potential was distributed on the S-MoO_2 nanosheet. The results mentioned above further proved that the photogenerated electrons of CdS-Cd were transferred to the S-MoO_2 nanosheet under light illumination, and the photogenerated holes remained on CdS-Cd particles. The surface potential and SPV images of CdS-Cd/S-MoO_2-75% with larger CdS particles in dark and under light more clearly proved the transfer path of photoinduced electrons and holes between CdS-Cd and S-MoO_2, as shown in Figure S17a,b.

4. CONCLUSIONS

In summary, the epitaxial growth of CdS-Cd nanopyramids on S-doped MoO_2 nanosheets (CdS-Cd/S-MoO_2) were prepared by cosublimation of CdS and MoO_3 at 900 °C under a reducing atmosphere of 10% H_2/Ar. MoO_2 nanosheets as supporting templates limited the size growth and induced the epitaxial growth of CdS-Cd nanopyramids. CdS-Cd/S-MoO_2-55% was composed of the CdS nanopyramids as photocatalysts and Cd and S-MoO_2 nanosheets as co-catalysts that showed efficient visible light-driven photocatalytic H_2 generation performance with a H_2 production rate of 24.98 μmol h^{-1} mg^{-1}, which was 11 times higher than that of the CdS-Cd nanoparticles (2.26 μmol h^{-1} mg^{-1}). Under the irradiation of visible light, the photogenerated electrons generated by CdS were transmitted to Cd and S-doped MoO_2, which reduced hydrogen ions to hydrogen molecules. The separation of the electron–hole pair and electronic transmission were confirmed by photoelectrochemical response, UPS and SPV, respectively. In other words, these findings provided a straightforward, large-scale, and practical way to produce cheap and efficient photocatalysts with cocatalysts.

■ ASSOCIATED CONTENT

Supporting Information

The Supporting Information is available free of charge at https://pubs.acs.org/doi/10.1021/acsami.9b17216.

DOI: 10.1021/acsami.9b17216
ACS Appl. Mater. Interfaces 2020, 12, 2362–2369

Experimental methods; the physical and SEM images of samples synthesized in large quantities; SEM-EDS of CdS-Cd/S-MoO_2 samples with different loading of CdS-Cd; EDS element mapping of Mo, O, and S in S-MoO_2; XRD and SEM of MoO_2 nanosheets; SEM image of CdS-Cd particles without MoO_2 nanosheets; XRD and SEM of CdS by the similar process in Ar gas; FESEM images and XRD of CdS-Cd/S-MoO2; CdS-Cd/S-MoO_2 that can be collected at the end of the quartz tube; AFM of the CdS-Cd/S-MoO_2-75%; the TEM mapping of CdS-Cd/S-MoO_2-75%; EDS element mapping of CdS-Cd/S-MoO_2-55%; PEC responses of CdS, CdS-Cd, S-MoO_2, MoO_2, CdS-Cd/S-MoO_2-55%, the fluorescence decay curves, and PL spectra of CdS, S-MoO_2, and CdS-Cd/S-MoO_2-55%; the photocatalyst hydrogen production of CdS, CdS-Cd, and 0.5 wt % Pt/CdS; the photocatalyst hydrogen production of MoO_2 and S-MoO_2; XRD and XPS of Mo 3d and Cd 3d; quantum efficiency (QE) and H_2 evolution amounts; the KPFM image of the surface potential distribution; quality statistics before and after dissolution of concentrated hydrochloric acid; and comparison of the photocatalytic hydrogen evolution activity of various catalysts (PDF)

AUTHOR INFORMATION

Corresponding Authors

*E-mail: mountainchu@163.com (B.C.).
*E-mail: hongliu@sdu.edu.cn (H.L.).
*E-mail: ifc_zhouwj@ujn.edu.cn (W. Z.).

ORCID

Hong Liu: 0000-0003-1640-9620
Weijia Zhou: 0000-0003-4339-0435

Notes

The authors declare no competing financial interest.

ACKNOWLEDGMENTS

This work was supported by the Fundamental Research Funds for Central Universities of SCUT (D2182400), the Tip-top Scientific and Technical Innovative Youth Talents of Guangdong Special Support Program (2016TQ03N541), the Guangdong Natural Science Funds for Distinguished Young Scholar (2017B030306001), the National Natural Science Foundation of China (91745203), and the Guangdong Innovative and Entrepreneurial Research Team Program (2014ZT05N200).

REFERENCES

(1) Fujishima, A.; Honda, K. Electrochemical Photolysis of Water at a Semiconductor Electrode. *Nature* **1972**, *238*, 37−38.

(2) Zhou, W.; Yin, Z.; Du, Y.; Huang, X.; Zeng, Z.; Fan, Z.; Liu, H.; Wang, J.; Zhang, H. Synthesis of Few-Layer MoS_2 Nanosheet-Coated TiO_2 Nanobelt Heterostructures for Enhanced Photocatalytic Activities. *Small* **2013**, *9*, 140−147.

(3) Tian, J.; Leng, Y.; Zhao, Z.; Xia, Y.; Sang, Y.; Hao, P.; Zhan, J.; Li, M.; Liu, H. Carbon quantum dots/hydrogenated TiO_2 nanobelt heterostructures and their broad spectrum photocatalytic properties under UV, visible, and near-infrared irradiation. *Nano Energy* **2015**, *11*, 419−427.

(4) Xiang, Q.; Yu, J.; Jaroniec, M. Synergetic Effect of MoS_2 and Graphene as Cocatalysts for Enhanced Photocatalytic H_2 Production Activity of TiO_2 Nanoparticles. *J. Am. Chem. Soc.* **2012**, *134*, 6575−6578.

(5) Yu, Y.; Nam, G.-H.; He, Q.; Wu, X.-J.; Zhang, K.; Yang, Z.; Chen, J.; Ma, Q.; Zhao, M.; Liu, Z.; Ran, F.-R.; Wang, X.; Li, H.; Huang, X.; Li, B.; Xiong, Q.; Zhang, Q.; Liu, Z.; Gu, L.; Du, Y.; Huang, W.; Zhang, H. High phase-purity 1T′-MoS_2- and 1T′-$MoSe_2$-layered crystals. *Nat. Chem.* **2018**, *10*, 638−643.

(6) Han, B.; Liu, S.; Zhang, N.; Xu, Y.-J.; Tang, Z.-R. One-dimensional CdS@MoS_2 core-shell nanowires for boosted photocatalytic hydrogen evolution under visible light. *Appl. Catal., B* **2017**, *202*, 298−304.

(7) Arif, M.; Zhang, M.; Yao, J.; Yin, H.; Li, P.; Hussain, I.; Liu, X. Layer-assembled 3D Bi_2WO_6 hierarchical architectures by Ti-doping for enhanced visible-light driven photocatalytic and photoelectrochemical performance. *J. Alloys Compd.* **2019**, *792*, 878−893.

(8) Guan, S.; Fu, X.; Zhang, Y.; Peng, Z. β-NiS modified CdS nanowires for photocatalytic H_2 evolution with exceptionally high efficiency. *Chem. Sci.* **2018**, *9*, 1574−1585.

(9) Bian, T.; Shang, L.; Yu, H.; Perez, M. T.; Wu, L.-Z.; Tung, C.-H.; Nie, Z.; Tang, Z.; Zhang, T. Spontaneous Organization of Inorganic Nanoparticles into Nanovesicles Triggered by UV Light. *Adv. Mater.* **2014**, *26*, 5613−5618.

(10) Shi, R.; Ye, H.-F.; Liang, F.; Wang, Z.; Li, K.; Weng, Y.; Lin, Z.; Fu, W.-F.; Che, C.-M.; Chen, Y. Interstitial P-Doped CdS with Long-Lived Photogenerated Electrons for Photocatalytic Water Splitting without Sacrificial Agents. *Adv. Mater.* **2018**, *30*, 1705941.

(11) Kim, Y. K.; Park, H. Light-harvesting multi-walled carbon nanotubes and CdS hybrids: Application to photocatalytic hydrogen production from water. *Energy Environ. Sci.* **2011**, *4*, 685−694.

(12) Xie, Y. P.; Yu, Z. B.; Liu, G.; Ma, X. L.; Cheng, H.-M. CdS−mesoporous ZnS core−shell particles for efficient and stable photocatalytic hydrogen evolution under visible light. *Energy Environ. Sci.* **2014**, *7*, 1895−1901.

(13) Han, S.; Hu, L.; Gao, N.; Al-Ghamdi, A. A.; Fang, X. Efficient Self-Assembly Synthesis of Uniform CdS Spherical Nanoparticles-Au Nanoparticles Hybrids with Enhanced Photoactivity. *Adv. Funct. Mater.* **2014**, *24*, 3725−3733.

(14) Ma, D.; Shi, J.-W.; Zou, Y.; Fan, Z.; Ji, X.; Niu, C.; Wang, L. Rational design of CdS@ZnO core-shell structure via atomic layer deposition for drastically enhanced photocatalytic H_2 evolution with excellent photostability. *Nano Energy* **2017**, *39*, 183−191.

(15) Sun, Q.; Wang, N.; Yu, J.; Yu, J. C. A Hollow Porous CdS Photocatalyst. *Adv. Mater.* **2018**, *30*, 1804368.

(16) Qiu, F.; Han, Z.; Peterson, J. J.; Odoi, M. Y.; Sowers, K. L.; Krauss, T. D. Photocatalytic Hydrogen Generation by CdSe/CdS Nanoparticles. *Nano Lett.* **2016**, *16*, 5347−5352.

(17) Jiang, Z.; Qian, K.; Zhu, C.; Sun, H.; Wan, W.; Xie, J.; Li, H.; Wong, P. K.; Yuan, S. Carbon nitride coupled with CdS-TiO_2 nanodots as 2D/0D ternary composite with enhanced photocatalytic H_2 evolution: A novel efficient three-level electron transfer process. *Appl. Catal., B* **2017**, *210*, 194−204.

(18) Wang, S.; Zhu, B.; Liu, M.; Zhang, L.; Yu, J.; Zhou, M. Direct Z-scheme ZnO/CdS hierarchical photocatalyst for enhanced photocatalytic H_2-production activity. *Appl. Catal., B* **2019**, *243*, 19−26.

(19) Arif, M.; Min, Z.; Yuting, L.; Yin, H.; Liu, X. A Bi_2WO_6-based hybrid heterostructures photocatalyst with enhanced photodecomposition and photocatalytic hydrogen evolution through Z-scheme process. *J. Ind. Eng. Chem.* **2019**, *69*, 345−357.

(20) Peng, T.; Li, K.; Zeng, P.; Zhang, Q.; Zhang, X. Enhanced Photocatalytic Hydrogen Production over Graphene Oxide−Cadmium Sulfide Nanocomposite under Visible Light Irradiation. *J. Phys. Chem. C* **2012**, *116*, 22720−22726.

(21) Tang, Z.-R.; Yin, X.; Zhang, Y.; Xu, Y.-J. Synthesis of Titanate Nanotube−CdS Nanocomposites with Enhanced Visible Light Photocatalytic Activity. *Inorg. Chem.* **2013**, *52*, 11758−11766.

(22) Shang, L.; Tong, B.; Yu, H.; Waterhouse, G. I. N.; Zhou, C.; Zhao, Y.; Tahir, M.; Wu, L.-Z.; Tung, C.-H.; Zhang, T. CdS Nanoparticle-Decorated Cd Nanosheets for Efficient Visible Light-Driven Photocatalytic Hydrogen Evolution. *Adv. Energy Mater.* **2016**, *6*, 1501241.

DOI: 10.1021/acsami.9b17216
ACS Appl. Mater. Interfaces 2020, 12, 2362−2369

(23) Xu, J.; Cao, X. Characterization and mechanism of MoS_2/CdS composite photocatalyst used for hydrogen production from water splitting under visible light. *Chem. Eng. J.* **2015**, *260*, 642−648.
(24) Chen, W.; Wang, Y.; Liu, M.; Gao, L.; Mao, L.; Fan, Z.; Shangguan, W. In situ photodeposition of cobalt on CdS nanorod for promoting photocatalytic hydrogen production under visible light irradiation. *Appl. Surf. Sci.* **2018**, *444*, 485−490.
(25) Zhang, J.; Liu, S.; Liang, H.; Dong, R.; Feng, X. Hierarchical Transition-Metal Dichalcogenide Nanosheets for Enhanced Electrocatalytic Hydrogen Evolution. *Adv. Mater.* **2015**, *27*, 7426−7431.
(26) Wu, A.; Tian, C.; Jiao, Y.; Yan, Q.; Yang, G.; Fu, H. Sequential two-step hydrothermal growth of MoS_2/CdS core-shell heterojunctions for efficient visible light-driven photocatalytic H_2 evolution. *Appl. Catal., B* **2017**, *203*, 955−963.
(27) Yang, L.; Zeng, L.; Liu, H.; Deng, Y.; Zhou, Z.; Yu, J.; Liu, H.; Zhou, W. Hierarchical microsphere of MoNi porous nanosheets as electrocatalyst and cocatalyst for hydrogen evolution reaction. *Appl. Catal., B* **2019**, *249*, 98−105.
(28) Zhu, Y.; Chen, Z.; Gao, T.; Huang, Q.; Niu, F.; Qin, L.; Tang, P.; Huang, Y.; Sha, Z.; Wang, Y. Construction of hybrid Z-scheme Pt/CdS−TNTAs with enhanced visible-light photocatalytic performance. *Appl. Catal., B* **2015**, *163*, 16−22.
(29) Kumar, D. P.; Hong, S.; Reddy, D. A.; Kim, T. K. Noble metal-free ultrathin MoS_2 nanosheet-decorated CdS nanorods as an efficient photocatalyst for spectacular hydrogen evolution under solar light irradiation. *J. Mater. Chem. A* **2016**, *4*, 18551−18558.
(30) Raja, R.; Sudhagar, P.; Devadoss, A.; Terashima, C.; Shrestha, L. K.; Nakata, K.; Jayavel, R.; Ariga, K.; Fujishima, A. Pt-free solar driven photoelectrochemical hydrogen fuel generation using 1T MoS_2 co-catalyst assembled CdS QDs/TiO_2 photoelectrode. *Chem. Commun.* **2015**, *51*, 522−525.
(31) Zhong, Y.; Zhao, G.; Ma, F.; Wu, Y.; Hao, X. Utilizing photocorrosion-recrystallization to prepare a highly stable and efficient CdS/WS_2 nanocomposite photocatalyst for hydrogen evolution. *Appl. Catal., B* **2016**, *199*, 466−472.
(32) Gopannagari, M.; Kumar, D. P.; Reddy, D. A.; Hong, S.; Song, M. I.; Kim, T. K. In situ preparation of few-layered WS_2 nanosheets and exfoliation into bilayers on CdS nanorods for ultrafast charge carrier migrations toward enhanced photocatalytic hydrogen production. *J. Catal.* **2017**, *351*, 153−160.
(33) Qin, N.; Xiong, J.; Liang, R.; Liu, Y.; Zhang, S.; Li, Y.; Li, Z.; Wu, L. Highly efficient photocatalytic H_2 evolution over MoS_2/CdS-TiO_2 nanofibers prepared by an electrospinning mediated photodeposition method. *Appl. Catal., B* **2017**, *202*, 374−380.
(34) Chen, J.; Wu, X.-J.; Yin, L.; Li, B.; Hong, X.; Fan, Z.; Chen, B.; Xue, C.; Zhang, H. One-pot Synthesis of CdS Nanocrystals Hybridized with Single-Layer Transition-Metal Dichalcogenide Nanosheets for Efficient Photocatalytic Hydrogen Evolution. *Angew. Chem. Int. Ed.* **2015**, *127*, 1226−1230.
(35) Jia, J.; Xiong, T.; Zhao, L.; Wang, F.; Liu, H.; Hu, R.; Zhou, J.; Zhou, W.; Chen, S. Ultrathin N-Doped Mo_2C Nanosheets with Exposed Active Sites as Efficient Electrocatalyst for Hydrogen Evolution Reactions. *ACS Nano* **2017**, *11*, 12509−12518.
(36) Lin, H.; Li, Y.; Li, H.; Wang, X. Multi-node CdS heteronanowires grown with defect-rich oxygen-doped MoS_2 ultrathin nanosheets for efficient visible-light photocatalytic H_2 evolution. *Nano Res.* **2017**, 1377−1392.
(37) Guo, L.; An, Q.; Xiao, Z.-Y.; Zhai, S.-R.; Cai, W.; Wang, H.; Li, Z. Constructing Stacked Structure of S-Doped Carbon Layer-Encapsulated MoO_2 NPs with Dominated Dielectric Loss for Microwave Absorption. *ACS Sustainable Chem. Eng.* **2019**, 19546.
(38) Tian, J.; Zhang, H.; Li, Z. Synthesis of Double-Layer Nitrogen-Doped Microporous Hollow Carbon@MoS2/MoO2 Nanospheres for Supercapacitors. *ACS Appl. Mater. Interfaces* **2018**, *10*, 29511−29520.
(39) Li, W.; Feng, C.; Dai, S.; Yue, J.; Hua, F.; Hou, H. Fabrication of sulfur-doped g-C_3N_4/Au/CdS Z-scheme photocatalyst to improve the photocatalytic performance under visible light. *Appl. Catal., B* **2015**, *168-169*, 465−471.
(40) Lei, Y.; Yang, C.; Hou, J.; Wang, F.; Min, S.; Ma, X.; Jin, Z.; Xu, J.; Lu, G.; Huang, K.-W. Strongly coupled CdS/graphene quantum dots nanohybrids for highly efficient photocatalytic hydrogen evolution: Unraveling the essential roles of graphene quantum dots. *Appl. Catal., B* **2017**, *216*, 59−69.
(41) Tan, C.; Zhang, H. Epitaxial Growth of Hetero-Nanostructures Based on Ultrathin Two-Dimensional Nanosheets. *J. Am. Chem. Soc.* **2015**, *137*, 12162−12174.
(42) Zhao, L.; Jia, J.; Yang, Z.; Yu, J.; Wang, A.; Sang, Y.; Zhou, W.; Liu, H. One-step synthesis of CdS nanoparticles/MoS_2 nanosheets heterostructure on porous molybdenum sheet for enhanced photocatalytic H_2 evolution. *Appl. Catal., B* **2017**, *210*, 290−296.
(43) Zhou, W.; Jia, J.; Lu, J.; Yang, L.; Hou, D.; Li, G.; Chen, S. Recent developments of carbon-based electrocatalysts for hydrogen evolution reaction. *Nano Energy* **2016**, *28*, 29−43.
(44) Seo, J. H.; Yang, R.; Brzezinski, J. Z.; Walker, B.; Bazan, G. C.; Nguyen, T.-Q. Electronic Properties at Gold/Conjugated-Polyelectrolyte Interfaces. *Adv. Mater.* **2009**, *21*, 1006−1011.
(45) Wu, X.; Zhao, J.; Wang, L.; Han, M.; Zhang, M.; Wang, H.; Huang, H.; Liu, Y.; Kang, Z. Carbon dots as solid-state electron mediator for $BiVO_4$/CDs/CdS Z-scheme photocatalyst working under visible light. *Appl. Catal., B* **2017**, *206*, 501−509.
(46) Zhu, J.; Fan, F.; Chen, R.; An, H.; Feng, Z.; Li, C. Direct Imaging of Highly Anisotropic Photogenerated Charge Separations on Different Facets of a Single $BiVO_4$ Photocatalyst. *Angew. Chem., Int. Ed.* **2015**, *54*, 9111−9114.
(47) Wang, H.; Gao, Y.; Liu, J.; Li, X.; Ji, M.; Zhang, E.; Cheng, X.; Xu, M.; Liu, J.; Rong, H.; Chen, W.; Fan, F.; Li, C.; Zhang, J. Efficient Plasmonic Au/CdSe Nanodumbbell for Photoelectrochemical Hydrogen Generation beyond Visible Region. *Adv. Eng. Mater.* **2019**, *9*, 1803889.

DOI: 10.1021/acsami.9b17216
ACS Appl. Mater. Interfaces 2020, 12, 2362−2369